Available online at www.sciencedirect.com
ScienceDirect
Journal of Sound and Vibration 314 (2008) 586–602
JOURNAL OF SOUND AND VIBRATION
www.elsevier.com/locate/jsvi

An improved method for restraining the end effect in empirical mode decomposition and its applications to the fault diagnosis of large rotating machinery

Fangji Wu*, Liangsheng Qu

State Key Laboratory for Manufacturing Systems Engineering, Research Institute of Diagnostics and Cybernetics, Xi'an Jiaotong University, Xi'an 710049, People's Republic of China

Received 21 November 2006; received in revised form 30 October 2007; accepted 5 January 2008
Handling Editor: L.G. Tham
Available online 14 February 2008

Abstract

The purpose of this paper is to introduce an improved slope-based method (ISBM) to restrain the end effect in empirical mode decomposition (EMD). With this method, non-stationary, nonlinear time series can be decomposed efficiently and accurately into a set of intrinsic mode functions (IMFs) and a residual trend. Furthermore, due to its robust end effect restraint ability, the ISBM provides an attractive alternative to the traditional end condition methods. For the purpose of mechanical fault diagnosis, the IMFs derived from the improved EMD are then used to extract the features of faults and remove the interference from environmental noise and some irrelevant components. Industrial case studies on large rotating machinery show that IMF derived from improved EMD is relatively easy to understand and especially useful for analysis of non-stationary, nonlinear time series.

1. Introduction

Empirical mode decomposition (EMD) is an adaptive and unsupervised method with which any complicated data set can be decomposed into a finite number of intrinsic mode functions (IMFs) within the time domain. Since this method bases purely on the properties observed in the data without appealing to the concept of stationarity, it is useful for analyzing non-stationary, nonlinear signals compared to other analysis methods like Fourier transforms and wavelet decomposition. Successful applications of this method have varied from rainfall analysis [1] to fault diagnosis of roller bearings [2].

Despite the success of this analysis tool, there are several issues that require further attention for effective application of EMD [3]. One of these issues is the end effect in EMD. The estimation of upper and lower envelopes as interpolated curves between extrema using cubic splines is a basic operation in EMD; then, how to construct the upper and lower envelopes that contain all the observed points just basing on the local

*Corresponding author.
E-mail address: wfj_ridc@sohu.com (F. Wu).

0022-460X/$ - see front matter © 2008 Elsevier Ltd. All rights reserved.
doi:10.1016/j.jsv.2008.01.020

maxima and local minima is important to the accurate decomposition result. If the envelopes are not well constructed, the ends of time series will oscillate wildly; then, the end infection will propagate inwards and corrupt the subsequent lower frequency IMFs [4]. So, finding appropriate end condition methods becomes a significant pursuit to EMD method researchers. In general, the task to handle this problem is essentially to use the known points of a signal to predict certain unknown points of the signal. If the signal is predictable in physics, the best method may be a model-based method, e.g., AR [5] or ANN [6] extension or prediction. However, these methods are not computationally acceptable since the sifting process of EMD needs large number of iterations. In this paper, an improved cubic spline end condition method based on the Dätig and Schlurmann's method is proposed and compared to other two traditional end condition methods. The present method turned out to work more effectively than the traditional methods and it is heavily recommended for future EMD applications.

Furthermore, the improved EMD is applied to the fault diagnosis of large rotating machinery. Large rotating machinery, such as steam turbines, gas turbines, turbine generators, and centrifugal compressors, is essential equipment in oil refineries, power plants, and chemical engineering plants. The efficient and accurate diagnosis of rotating machinery is an important part of maintenance program to reduce operating and maintenance costs [7,8]. Along with the development of signal processing, more and more signal processing tools have been introduced to diagnose the faults in rotating machinery. This paper focuses on the IMFs derived from the improved EMD to extract the features of faults. By this means, the interference from environmental noise and some irrelevant components are removed. Moreover, this kind of IMFs are relatively easy to understand and especially useful for analysis of non-stationary, nonlinear time series.

For a clear presentation, this paper is organized as follows. In Section 2, the EMD algorithm is briefly introduced. After the review of other two traditional end condition methods, the improved method to restrain the end effect in EMD is presented in Sections 3. Section 4 shows the effect when the improved EMD is applied to numerical simulation examples. Then, in Section 5 the IMFs derived from improved EMD are used to analyze non-stationary, nonlinear signals of large rotating machinery. Finally, conclusions are stated in Section 6.

2. Empirical mode decomposition

EMD method introduced by Huang et al. is a relatively new time series analysis tool in comparison with traditional methods such as Fourier methods, wavelet methods, and empirical orthogonal functions. A signal will be broken down into its component IMFs by EMD. An IMF is a function that satisfies two conditions: (1) the number of local extrema and the number of zero crossings must be equal or differ by 1 at most; (2) at any point the mean value of the envelope defined by the local maxima and the envelope defined by the local minima must be zero.

For a signal $x(t)$, IMFs can be obtained by using the following sifting process:

(1) Initialize: $r_0(t) = x(t)$, and $i = 1$.
(2) Extract the ith IMF:
   a. initialize: $h_0(t) = r_{i-1}(t)$, $k = 1$;
   b. extract the local maxima and minima of $h_{k-1}(t)$;
   c. interpolate the local maxima and the local minima by a cubic spline to form upper and lower envelopes of $h_{k-1}(t)$;
   d. calculate the mean $m_{k-1}(t)$ of the upper and lower envelopes of $h_{k-1}(t)$;
   e. create: $h_k(t) = h_{k-1}(t) - m_{k-1}(t)$; and
   f. if stopping criterion is satisfied then set $h_k(t) = \mathrm{IMF}_i(t)$. Else go to b. with $k = k+1$.
(3) Define: $r_i(t) = r_{i-1}(t) - \mathrm{IMF}_i(t)$.
(4) If $r_i(t)$ still has at least 2 extrema then go to (2) with: $i = i+1$ else the decomposition is finished and $r_i(t)$ is the residue of the data set.

The result of the sifting process is a set of very nearly orthogonal functions, and the number of functions in the set depends on the original signal.

3. Cubic spline end condition methods

The first method for dealing with the spline end conditions proposed by Huang et al. [4] and slightly modified by Coughlin and Tung [9] is to pad the beginning and the end of the time series with additional "characteristic" or "typical" waves. Huang et al. based their additional waves on the two closest maxima and minima, while Coughlin and Tung based theirs on the closest maximum and minimum. A simpler method proposed and tested by Rilling et al. [10] is to "mirrorize" the extrema closest to the edge, rather than pad the time series with extra data. Chiew et al. [11] used the average of the two closest maxima (minima) for the maximum (minimum) spline. Dätig and Schlurmann [12] proposed a method based on the slopes of maxima and minima near both ends of the data series. All the above methods try to add boundary extrema by simple methods to represent characteristic natural behaviors of the original time series.

3.1. The mirror method

The mirror method (MM) proposed by Rilling et al. is to add extrema by mirror symmetry with respect to the extrema that are closest to the edges.

For the time series $x(t)$ as shown in Fig. 1, the procedure that the MM works is shown below:

(1) Find the extremum closest to the left edge of time series; thus we obtain Max(1). Then, find the extremum closest to Max(1); thus we obtain Min(1).
(2) Find the extremum closest to the right edge of time series; thus we obtain Min(N). Then, find the extremum closest to Min(N); thus we obtain Max(N) (shown in Fig. 1).
(3) For the left edge of time series, add minimum by mirror symmetry with respect to the maximum closest to the left edge; thus we obtain Min(0).
(4) For the right edge of time series, add maximum by mirror symmetry with respect to the minimum closest to the right edge; thus we obtain Max(N+1) (shown in Fig. 2).

The newly obtained Min(0) and Max(N+1) are then taken for construction of the upper and lower envelopes along with initial extrema as shown in Fig. 2.

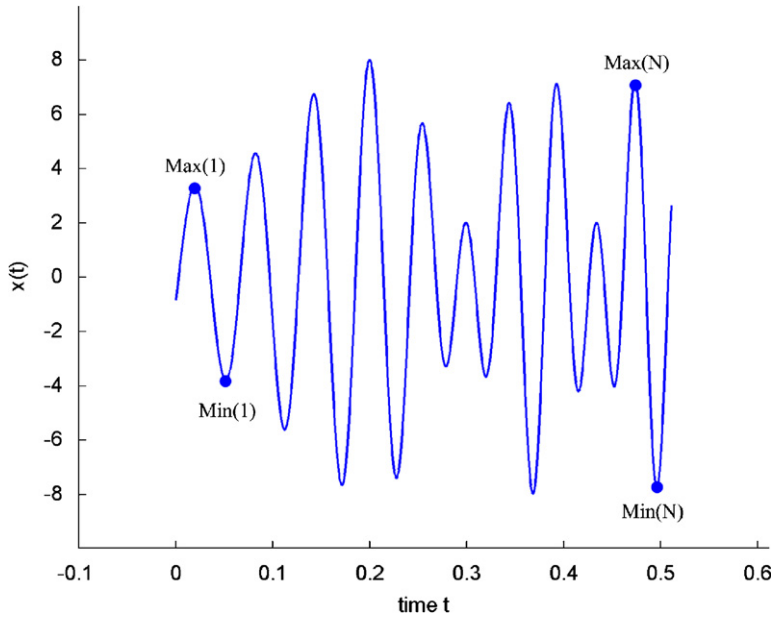

Fig. 1. The time series $x(t)$.

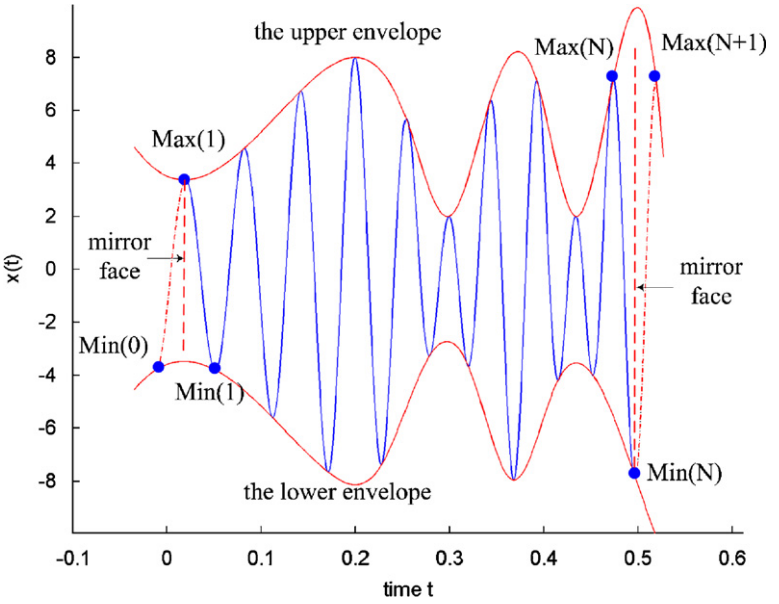

Fig. 2. The illustration of the mirror method.

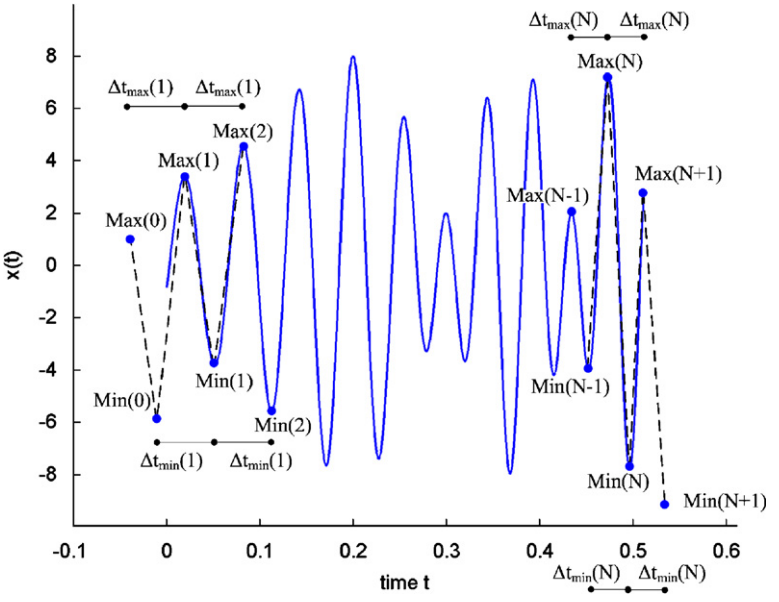

Fig. 3. The illustration of the slope-based method.

3.2. The slope-based method

The slope-based method (SBM) is proposed by Dätig and Schlurmann. This method is principally shown in Fig. 3. By this extended method, new maxima and minima of the data series are generated using two mathematically defined slopes created through the data itself. These gradients represent a kind of natural steepness derived from amplitude differences and distances between successive minima and maxima.

For the time series $x(t)$ as shown in Fig. 1, let $U(i)$ and $u(i)$ be the ordinate and abscissa values of the ith maximum Max(i); let $V(i)$ and $v(i)$ be the ordinate and abscissa values of the ith minimum Min(i). Fig. 3

considers the case when a maximum is the first extremum in the front of a signal. Then slope $s1$ is defined as

$$s1 = \frac{U(2) - V(1)}{u(2) - v(1)} \tag{1}$$

and slope $s2$ is given by

$$s2 = \frac{V(1) - U(1)}{v(1) - u(1)}. \tag{2}$$

Then, the time gaps between the first two successive maxima and minima are determined as $\Delta t_{\max}(1) = u(2) - u(1)$ and $\Delta t_{\min}(1) = v(2) - v(1)$. The new boundary extrema Min(0) and Max(0) are newly defined and shifted according to the corresponding time gaps $\Delta t_{\min}(1)$ and $\Delta t_{\max}(1)$, and gradients $s1$ and $s2$. The abscissa coordinates of the new extrema are located at

$$\begin{aligned} v(0) &= v(1) - \Delta t_{\min}(1), \\ u(0) &= u(1) - \Delta t_{\max}(1). \end{aligned} \tag{3}$$

While the ordinate coordinates of these new boundary knots are positioned at

$$\begin{aligned} V(0) &= U(1) - s1(u(1) - v(0)), \\ U(0) &= V(0) - s2(v(0) - u(0)). \end{aligned} \tag{4}$$

This procedure has to be similarly repeated for the generation of additional boundary knots at the end of the data series, which considers the case when a minimum is the last extremum. After having determined the time gaps between the last two successive maxima and minima at the rear of the signal $\Delta t_{\max}(N) = u(N) - u(N-1)$ and $\Delta t_{\min}(N) = v(N) - v(N-1)$, the corresponding slope $s3$ is defined as

$$s3 = \frac{V(N) - U(N)}{v(N) - u(N)} \tag{5}$$

and slope $s4$ is given by

$$s4 = \frac{U(N) - V(N-1)}{u(N) - v(N-1)}. \tag{6}$$

The new boundary extrema Max($N+1$) and Min($N+1$) are newly defined and shifted according to the corresponding time gaps $\Delta t_{\max}(N)$ and $\Delta t_{\min}(N)$, and gradients $s4$ and $s3$. The abscissa coordinates of the new extrema are located at

$$\begin{aligned} u(N+1) &= u(N) + \Delta t_{\max}(N), \\ v(N+1) &= v(N) + \Delta t_{\min}(N). \end{aligned} \tag{7}$$

While the ordinate coordinates of these new boundary knots are positioned at

$$\begin{aligned} U(N+1) &= V(N) + s4(u(N+1) - v(N)), \\ V(N+1) &= U(N+1) + s3(v(N+1) - u(N+1)). \end{aligned} \tag{8}$$

The newly obtained Min(0), Max(0), Min($N+1$), and Max($N+1$) are then taken for construction of the upper and lower envelopes along with initial extrema.

In fact, the SBM can sometimes make the ends of time series oscillate wildly although it turns out to work quite successfully for most purposes of the analysis of non-stationary, nonlinear time series.

Fig. 4 describes a counterexample of the application of SBM to non-stationary, nonlinear time series. In Fig. 4, $x(1)$ is the first point of the time series and $x(N)$ is the last point of the time series. The upper and lower envelopes constructed by using the newly obtained Min(0), Max(0), Min($N+1$), and Max($N+1$) fail to contain all points; the ends of time series will then oscillate wildly. Furthermore, the end infection will propagate inwards and corrupt the subsequent lower-frequency IMFs with this SBM.

In order to improve the SBM to obtain an efficient and accurate EMD algorithm, a new method is proposed below. With this improved method, the end effect in EMD can be restrained more successfully.

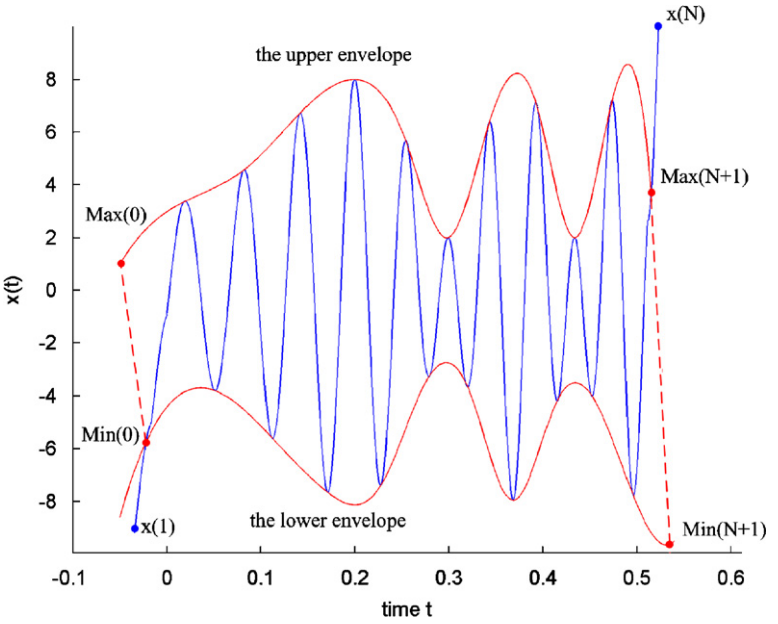

Fig. 4. The counterexample of the application of slope-based method.

3.3. The improved slope-based method (ISBM)

The SBM utilizes the characteristic steepness of the data itself and possesses simple methodology. However, it fails to consider some conditions as the first calculated maximum (minimum) is less (larger) than the first point in the front or the last point at the end of the signal (see Fig. 4). These cases may occur when the data consists of intrinsic mode oscillations of far different magnitude or time scale. The envelopes constructed by using the SBM will exclude several points of the signal in these cases, and the ends of time series will then oscillate wildly during the sifting process. In order to get a more efficient measure, the ISBM is proposed below.

For time series $x(t)$, let $U(i)$ and $u(i)$ be the ordinate and abscissa values of the ith maximum Max(i); let $V(i)$ and $v(i)$ be the ordinate and abscissa values of the ith minimum Min(i). Also, the time gaps between the first two successive maxima and minima are determined as $\Delta t_{\max}(1) = u(2) - u(1)$ and $\Delta t_{\min}(1) = v(2) - v(1)$; the time gaps between the last two successive maxima and minima are $\Delta t_{\max}(N) = u(N) - u(N-1)$ and $\Delta t_{\min}(N) = v(N) - v(N-1)$. The ISBM can be described as following algorithm:

(1) Calculate the additional boundary data points for $x(t)$ according to the SBM introduced above.
(2) If a maximum is the first extremum in the front of $x(t)$, compare newly obtained Min(0) to the first point of the time series $x(1)$
   a. If Min(0) $> x(1)$, replace Min(0) with $x(1)$ as the first additional minimum; then, locate the first additional maximum Max(0) at

$$u(0) = u(1) - \Delta t_{\max}(1)$$
$$U(0) = V(0) - \frac{V(1) - U(1)}{v(1) - u(1)}(v(0) - u(0)). \tag{9}$$

   b. Else continue
(3) If a minimum is the first extremum in the front of $x(t)$, compare newly obtained Max(0) to the first point of the time series $x(1)$

a. If $\mathrm{Max}(0)<x(1)$, replace Max(0) with $x(1)$ as the first additional maximum; then, locate the first additional minimum Min(0) at

$$v(0) = v(1) - \Delta t_{\min}(1)$$
$$V(0) = U(0) - \frac{U(1) - V(1)}{u(1) - v(1)}(u(0) - v(0)). \tag{10}$$

b. Else continue

(4) If a maximum is the first extremum on the rear side of $x(t)$, compare newly obtained $\mathrm{Min}(N+1)$ to the last point of the time series $x(N)$

a. If $\mathrm{Min}(N+1)>x(N)$, replace $\mathrm{Min}(N+1)$ with $x(N)$ as the last additional minimum; then, locate the last additional maximum $\mathrm{Max}(N+1)$ at

$$u(N+1) = u(N) + \Delta t_{\max}(N)$$
$$U(N+1) = V(N+1) + \frac{U(N) - V(N)}{u(N) - v(N)}(u(N+1) - v(N+1)). \tag{11}$$

b. Else continue

(5) If a minimum is the last extremum on the rear side of $x(t)$, compare newly obtained $\mathrm{Max}(N+1)$ to the last point of the time series $x(N)$

a. If $\mathrm{Max}(N+1)<x(N)$, replace $\mathrm{Max}(N+1)$ with $x(N)$ as the last additional maximum; then, locate the last additional minimum $\mathrm{Min}(N+1)$ at

$$v(N+1) = v(N) + \Delta t_{\min}(N)$$
$$V(N+1) = U(N+1) + \frac{V(N) - U(N)}{v(N) - u(N)}(v(N+1) - u(N+1)). \tag{12}$$

b. Else continue

(6) End.

An example of this method used for time series is shown in Fig. 5. This new method takes advantage of the SBM to utilize the characteristic steepness of the data itself. Moreover, it turned out to work more effectively than the SBM.

4. Numerical simulation comparison

In this section, three end condition methods introduced above are compared by investigating the orthogonality of IMFs of several numerical simulation time series. Let Ort be the orthogonality of IMFs of a time series $x(t)$:

$$\mathrm{Ort} = \frac{1}{2}\sum_{i=1}^{n}\sum_{j=1}^{n}\left|\mathrm{IMF}(i)\mathrm{IMF}(j)\Big/\sum_{t}x^2(t)\right| \quad (i\neq j), \tag{13}$$

where IMF(i) and IMF(j) are the ith IMF and jth IMF of $x(t)$. The value of Ort represents the property of orthogonality and a small Ort value means good orthogonality that IMFs of the time series possess.

By virtue of the decomposition, the IMFs should all be locally orthogonal to each other, for each IMF is obtained from the difference between the signal and its local mean through the maximal and minimal envelopes; therefore [4],

$$\overline{(x(t) - \overline{x(t)})\,\overline{x(t)}} = 0. \tag{14}$$

Since the mean here is not the true mean, but a local mean of the envelopes defined by the local extrema, Eq. (14) is not strictly true and leakage should be small. However, if the end condition method behaves

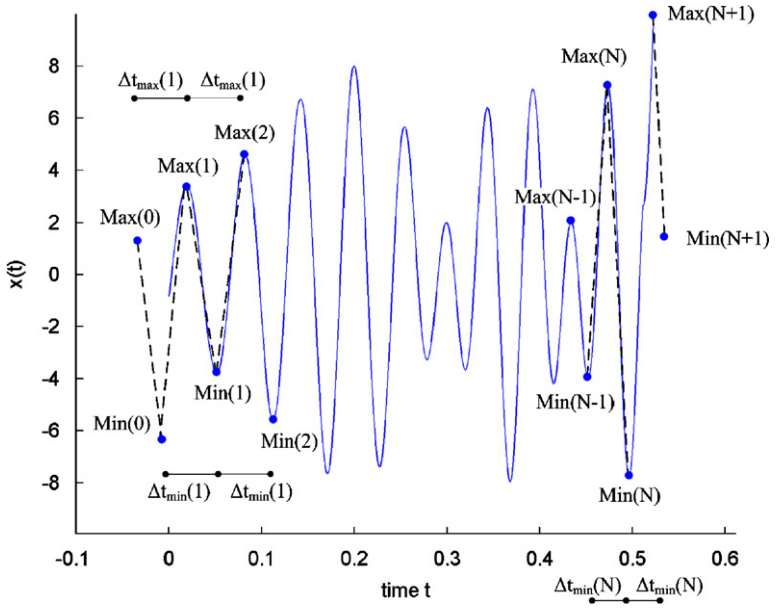

Fig. 5. The illustration of the improved slope-based method.

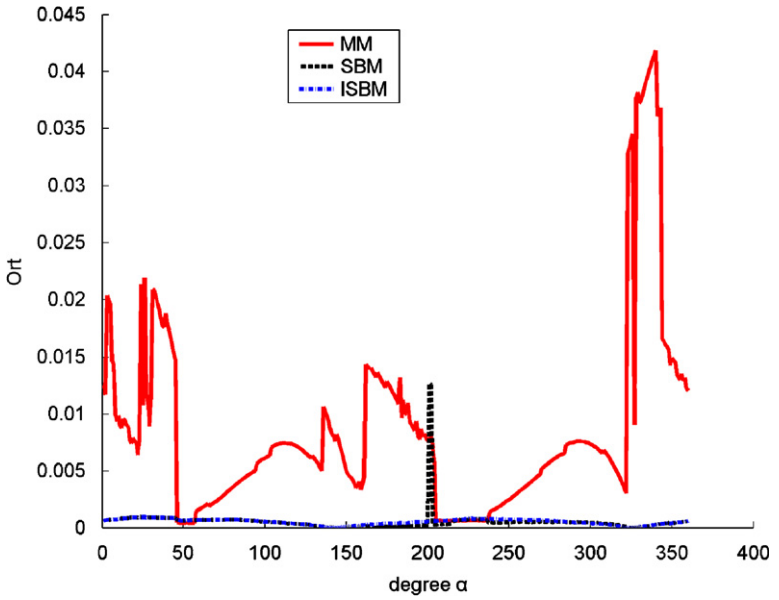

Fig. 6. Contrast among MM, SBM, and ISBM for $x_a(t)$.

inefficiently and envelopes are not well constructed, the ends of time series will oscillate wildly and the local mean will distance much more from the true mean which causes the Ort value to increase accordingly. So, the Ort value is employed to compare different methods as the criterion in this paper.

The first numerical example is given by

$$x_\alpha(t) = \cos(2\pi(30 + 6t)\,t) + \cos(4\pi t - \alpha\,\pi/180), \tag{15}$$

with $\alpha = 1,2,\ldots,360$. All these time series include frequency modulation (FM) signal components.

The contrast among MM, SBM, and ISBM is shown in Fig. 6. We can observe in this figure that SBM and ISBM behave much better than MM. Furthermore, we can notice that ISBM is better than SBM because of its

robust end effect restraint ability by comparison between SBM and ISBM as shown in Fig. 7. By observing Fig. 7, we then use EMD to analyze the signal:

$$x_{201}(t) = \cos(2\pi(30 + 6t)\,t) + \cos(4\pi t - 201\pi/180). \tag{16}$$

The result of EMD to $x_{201}(t)$ using SBM and ISBM is shown in Fig. 8, from which we can see that ISBM can decompose this time series more efficiently and accurately into a set of IMFs than SBM.

The second numerical example is given by

$$y_{\alpha}(t) = \cos(2\pi(30 + 6t)\,t - \alpha\,\pi/180) + 2\,\cos(2\pi t - \alpha\,\pi/180), \tag{17}$$

with $\alpha = 1,2,\ldots,360$.

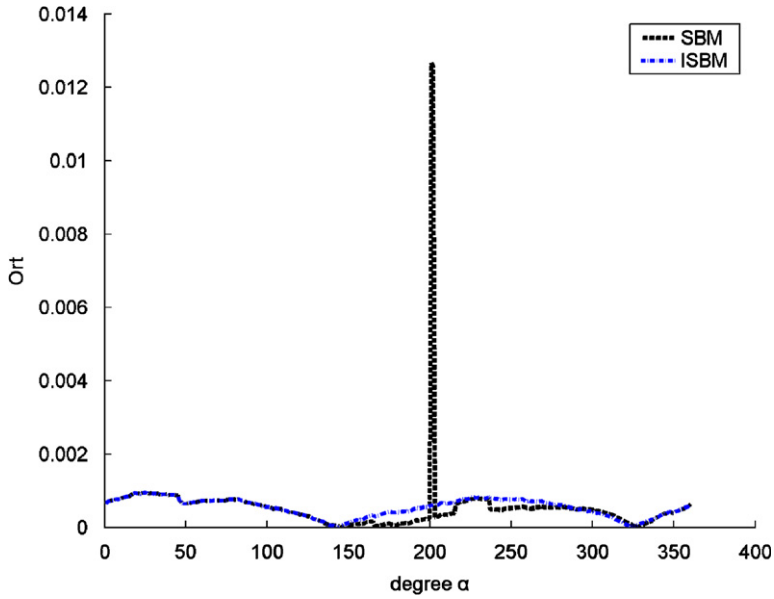

Fig. 7. Comparison between SBM and ISBM for $x_{\alpha}(t)$.

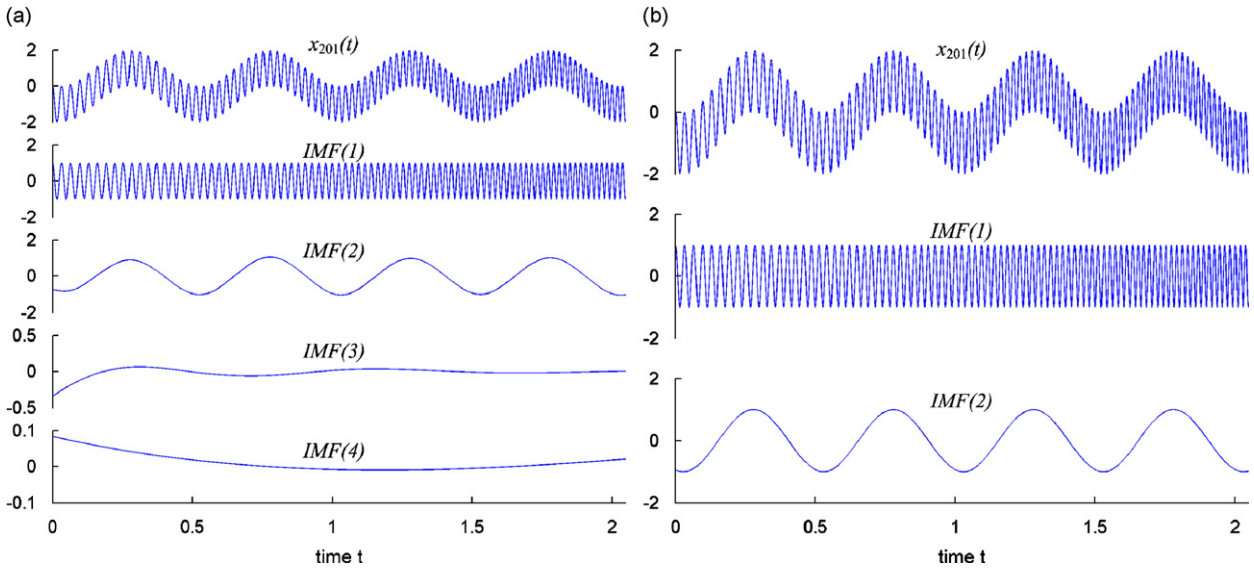

Fig. 8. The result of EMD to $x_{201}(t)$: (a) using SBM, (b) using ISBM.

The Ort values according to three different end condition methods for time series $y_\alpha(t)$ with $\alpha = 1,2,\ldots,360$ are shown in Fig. 9. From this figure, we can conclude that MM and ISBM are better than SBM for these time series. Then, by further contrast between MM and ISBM as shown in Fig. 10, we can see that ISBM is much better than MM because the Ort values obtained by using ISBM are much smaller than MM. Then, by observing Fig. 10, we use EMD to analyze the signal:

$$y_{196}(t) = \cos(2\pi(30 + 6t)\,t - 196\pi/180) + 2\cos(2\pi t - 196\pi/180). \tag{18}$$

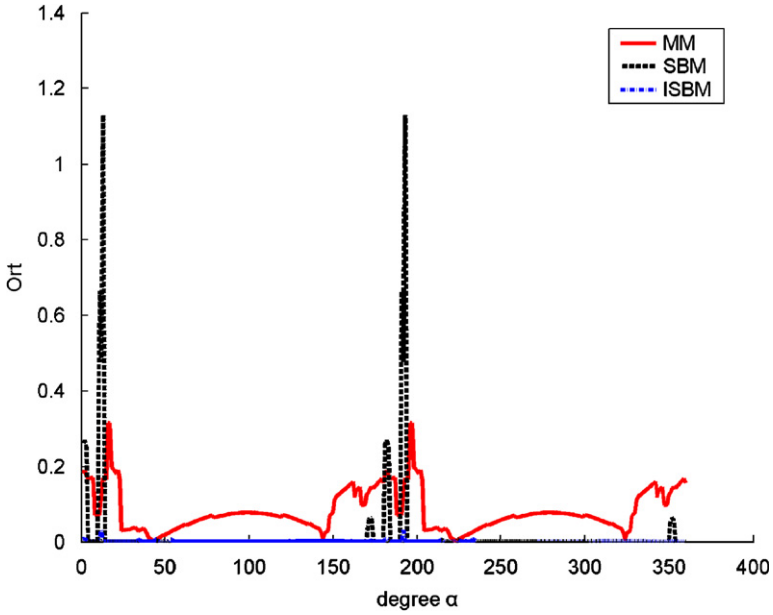

Fig. 9. Contrast among MM, SBM, and ISBM for $y_\alpha(t)$.

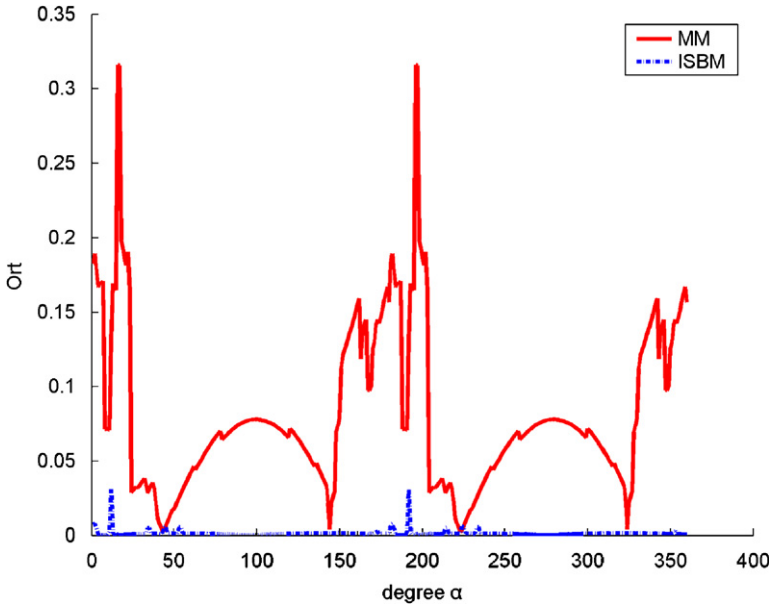

Fig. 10. Contrast between MM and ISBM for $y_\alpha(t)$.

The result of EMD to $y_{196}(t)$ using MM and ISBM is shown in Fig. 11. From this figure we can see that ISBM can decompose this time series more efficiently and accurately into a set of IMFs than MM.

The last synthetic example is

$$z_\alpha(t) = \cos(40\pi t - \alpha\pi/180) + 3\cos(10\pi t + \alpha\pi/180) + 5\cos(2\pi t + \alpha\pi/180), \tag{19}$$

with $\alpha = 1,2,\ldots,360$. All these time series consist of three sine signal components.

Fig. 12 shows the Ort values for time series $z_\alpha(t)$ with $\alpha = 1,2,\ldots,360$ according to MM, SBM, and ISBM. We can see from this figure that ISBM is much better than MM and SBM for these time series consist of sine signals. By further comparison between SBM and ISBM as shown in Fig. 13, we can conclude that ISBM has

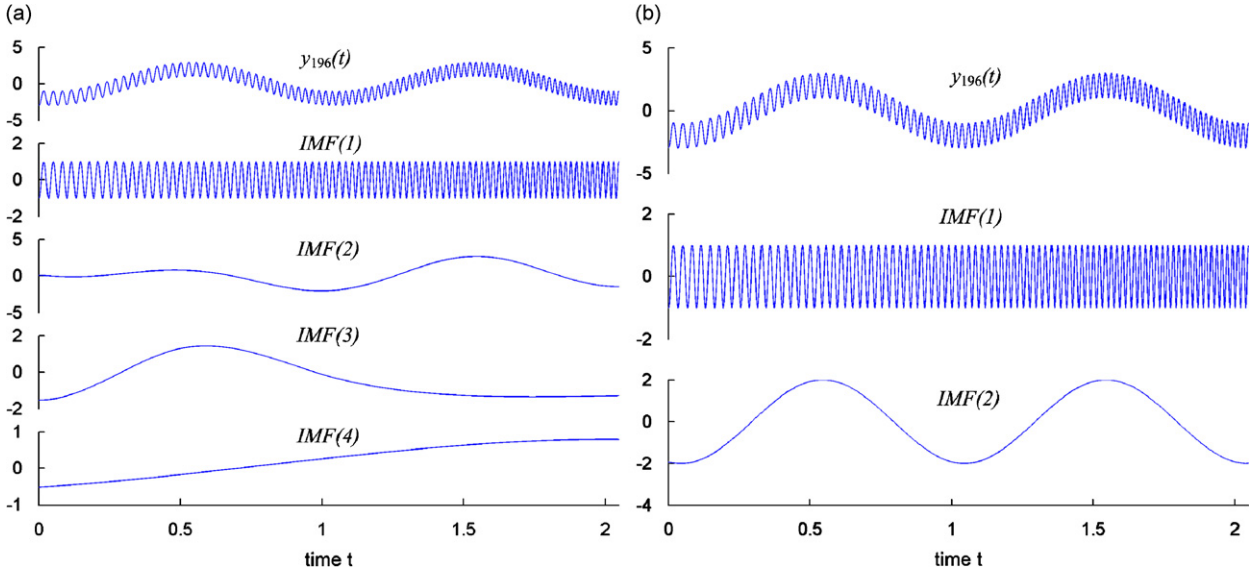

Fig. 11. The result of EMD to $y_{196}(t)$: (a) using MM, (b) using ISBM.

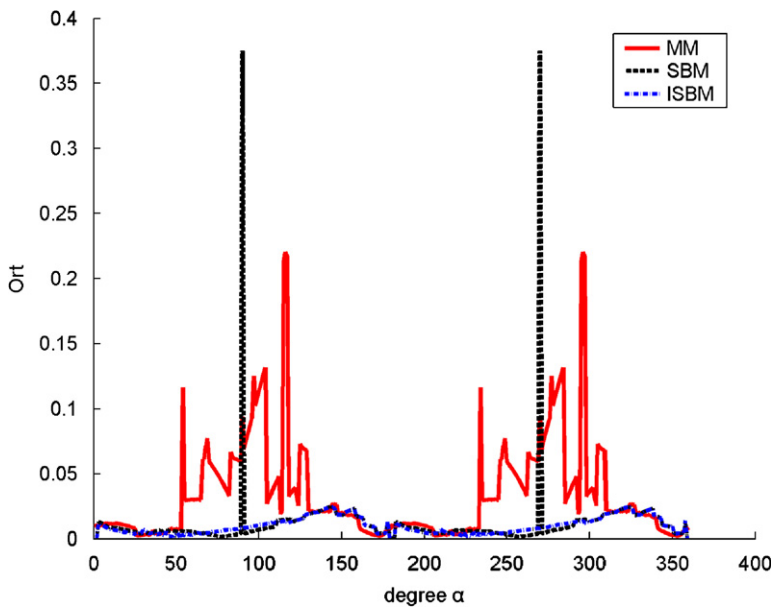

Fig. 12. Contrast among MM, SBM, and ISBM for $z_\alpha(t)$.

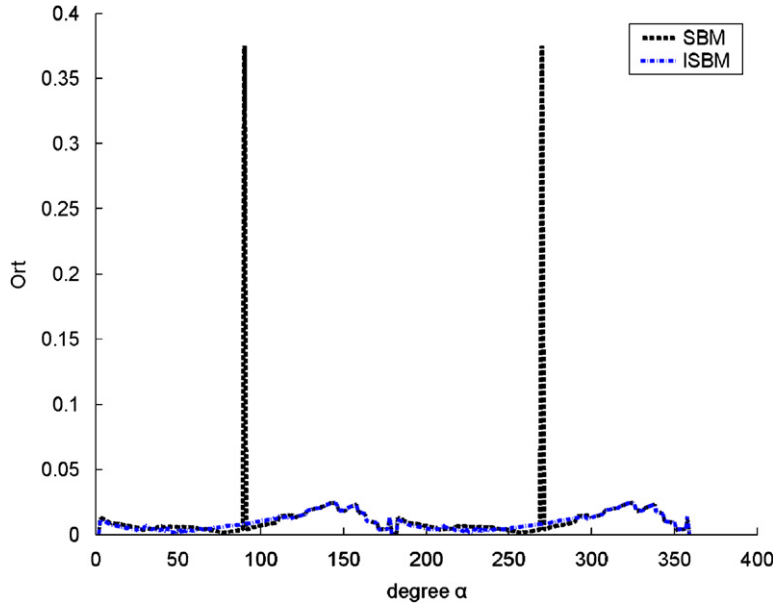

Fig. 13. Comparison between SBM and ISBM for $z_a(t)$.

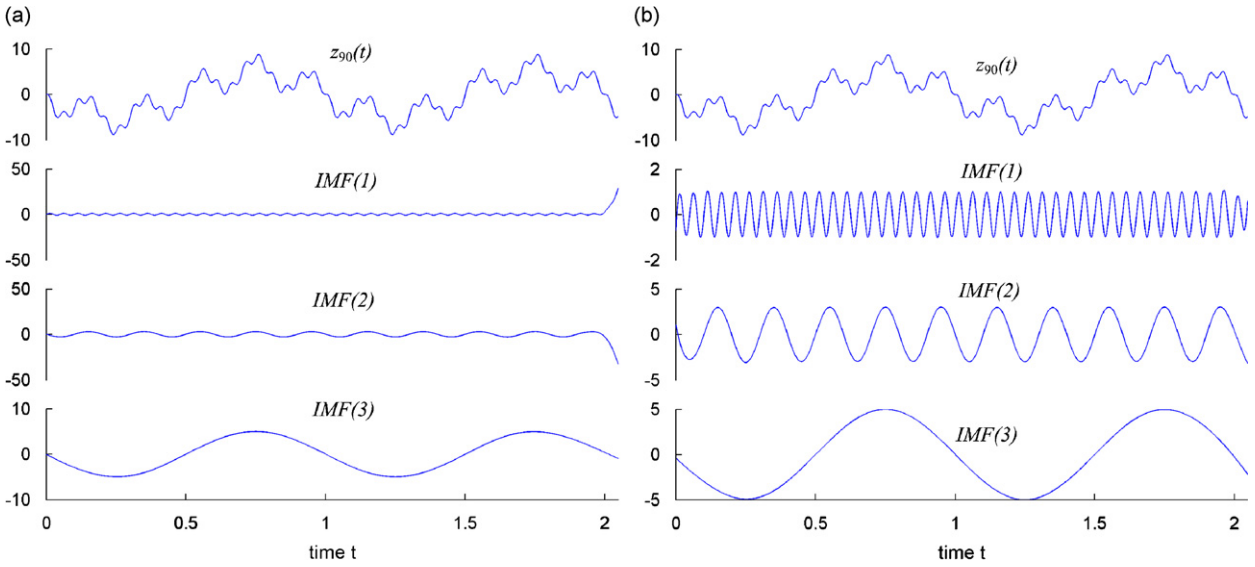

Fig. 14. The result of EMD to $z_{90}(t)$: (a) using SBM, (b) using ISBM.

robust end effect restraint ability than SBM. Then, by observing Fig. 13, we use EMD to analyze the signal:

$$z_{90}(t) = \cos(40\pi t - 90\pi/180) + 3\cos(10\pi t + 90\pi/180) + 5\cos(2\pi t + 90\pi/180). \quad (20)$$

The result of EMD to $z_{90}(t)$ using SBM and ISBM is shown in Fig. 14, from which we can see that ISBM can decompose this time series more efficiently and accurately into a set of IMFs than SBM. All the three sine components are decomposed completely by ISBM.

Through three simulation examples described above, we can find that the present method turned out to work quite successfully on numerical simulation signals and can be regarded as a technical improvement of the numerical sifting process of the EMD.

5. Applications of the ISBM to fault diagnosis of large rotating machinery

In this section, industrial case studies on large rotating machinery are presented to show the efficiency of the diagnosis approach based on the IMFs derived from improved EMD with ISBM. The vibration displacements are collected using eddy current proximity probe with a sensitivity of 200 mV/mil. Each data set consists of 1024 data points and is sampled at a rate of 2000 Hz.

Taking advantage of EMD, the newly obtained IMFs remove the interference from environmental noise and some irrelevant components for fault diagnosis. Each IMF contains an oscillatory mode inherent at a different narrow range of spatial frequencies.

The radial rub between the rotor and stator of the machine is a serious malfunction that may lead to catastrophic failure. The rub normally involves several physical effects, such as friction, impacting, and nonlinear behaviors in the rotor-bearing system. The rub signals in the FFT spectrum will show several super-harmonic components besides the synchronous vibration components. Fig. 15 shows FFT spectra of two practical signals from the horizontal and vertical sensors set in one measuring plane of a gas turbine. The Ort values of these two signals with MM, SBM, and ISBM are tabulated in Table 1. It can be seen that ISBM works better than MM and SBM; the IMFs of these two signals possess better orthogonality with ISBM than other two end condition methods.

Fig. 16 shows IMFs and residual trends of these two practical signals derived from improved EMD with ISBM. Then, the orbit is reconstructed based on the improved EMD to extract the feature of radial rub and remove the interference from environmental noise and some irrelevant components by discarding those IMFs with less persistent high-frequency components (Fig. 17). We can observe in Fig. 17 that shaft orbit suddenly

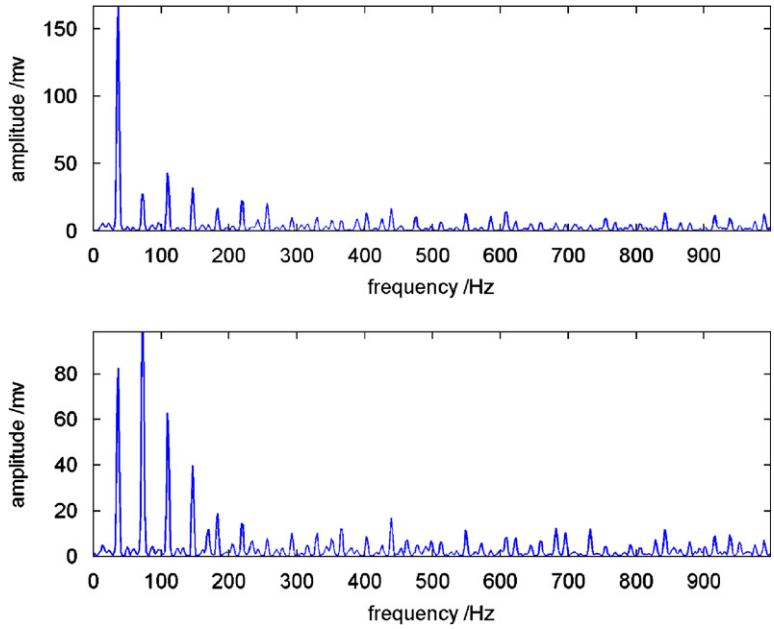

Fig. 15. FFT spectra: (a) signal from horizontal sensor, (b) signal from vertical sensor.

Table 1
The Ort values of two signals from gas turbine with MM, SBM, and ISBM

	MM	SBM	ISBM
Signal from horizontal sensor $h(t)$	0.052677	1.0555	0.047821
Signal from vertical sensor $v(t)$	0.16184	1.8652	0.13731

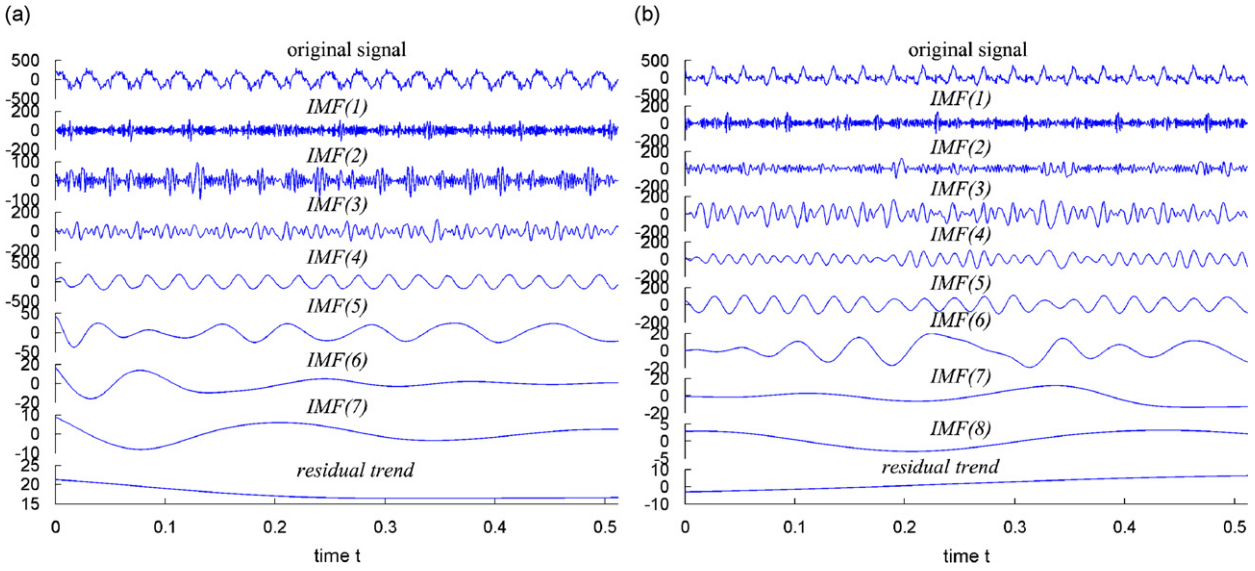

Fig. 16. IMFs and residual trends: (a) signal from horizontal sensor, (b) signal from vertical sensor.

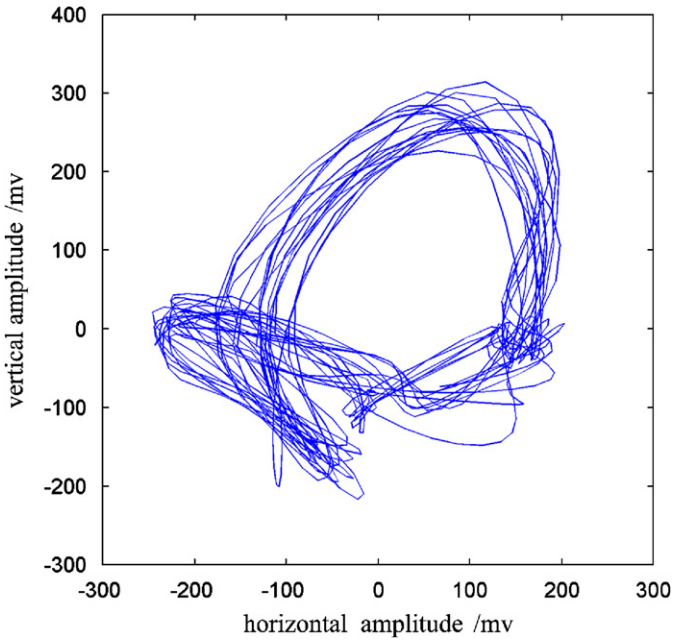

Fig. 17. Reconstructed shaft orbit.

changed its elliptical trajectory causing by radial rub between the rotor and stator. So, acute change of curvature of shaft orbit can be noticed and considered as a feature of the radial rub.

Fig. 18 shows the FFT spectrum of a signal from the compressor. This spectrum shows a large synchronous vibration component with a half-synchronous vibration component. The Ort values of this signal with MM, SBM, and ISBM are tabulated in Table 2. It can be seen from this table that the Ort value with ISBM is smallest of all the three end condition methods.

From Fig. 18 we may deduce that this compressor can be involved in Oil whirl or rotating stall. However, when this signal is decomposed into IMFs using the improved EMD with ISBM as shown in Fig. 19, another

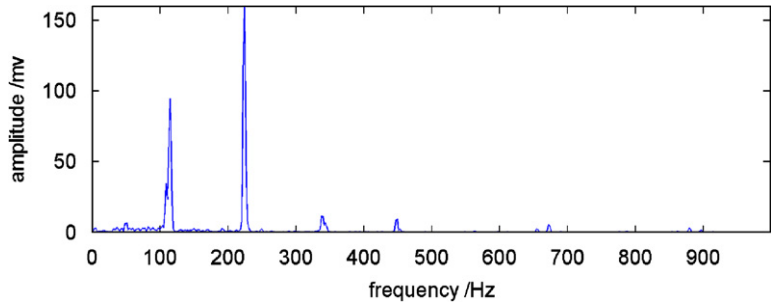

Fig. 18. FFT spectrum of a signal from the compressor.

Table 2
The Ort values of signal from compressor with MM, SBM, and ISBM

	MM	SBM	ISBM
Signal from compressor	0.040154	2.7417	0.03747

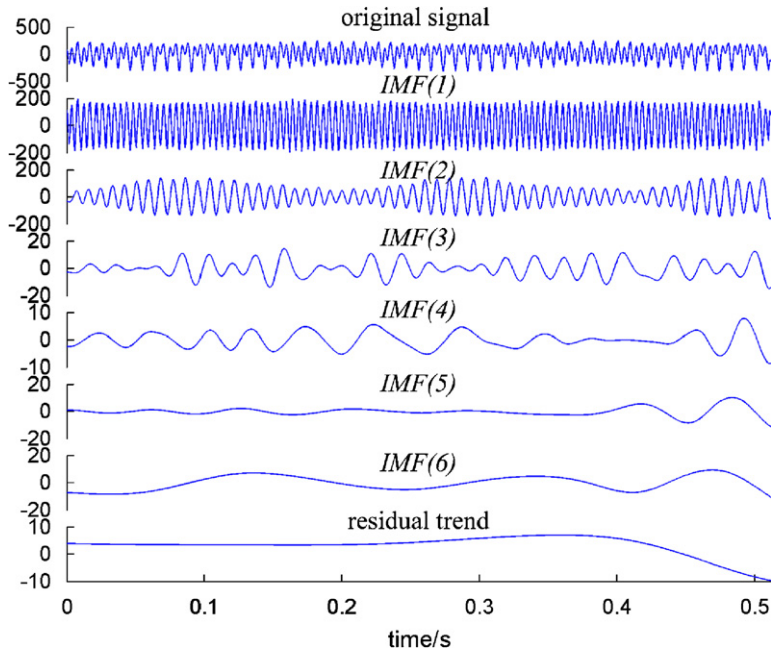

Fig. 19. IMFs and residual trend of signal from the compressor.

perspective may emerge. We can easily see from this figure that this signal from the compressor contains an amplitude modulation component. By further study of this amplitude modulation signal as IMF(2) shown in Fig. 19, we can see that it was caused by amplitude modulation of a 2.5 Hz component to the half-synchronous vibration component (112 Hz). Further inspection indicated that the 2.5 Hz component was caused by abnormal pipe excitation. After solving this fault caused by abnormal pipe excitation, the vibration decreased obviously. The spectra of IMF(1) and IMF(2) are shown in Fig. 20, from which we can see that the FFT spectrum of signal from the compressor primarily consist of spectrum of IMF(1) and IMF(2). In fact, one can

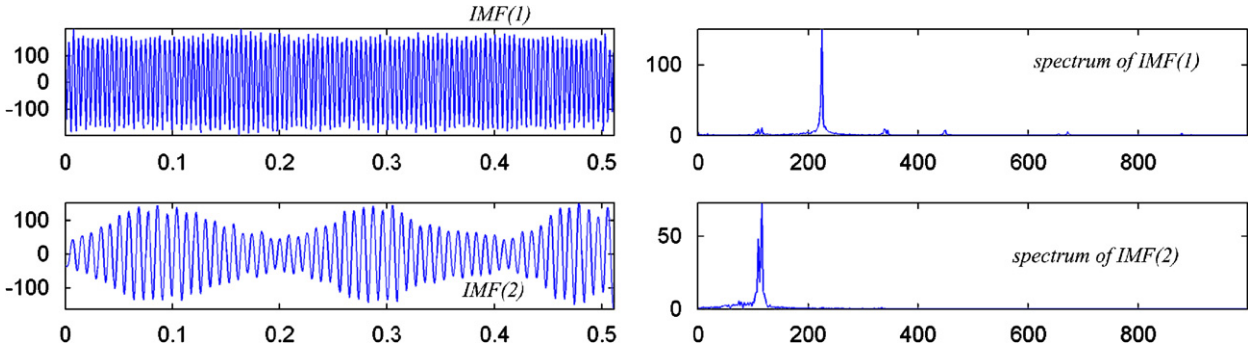

Fig. 20. FFT spectra of IMF(1) and IMF(2).

notice the fault by careful and prudent observation on FFT spectrum. However, EMD provides an easier and clearer approach to this fault diagnosis. So, without investigation of the signal in time domain by IMFs derived from the improved EMD, an inaccurate diagnosis may be stated.

Through the cases described above, the efficiency of the diagnosis approach based on the IMFs derived from improved EMD with ISBM to non-stationary, nonlinear signals can be manifested. Moreover, this kind of IMFs is relatively easy to understand and especially useful for analysis of non-stationary, nonlinear time series. Furthermore, the improved EMD can also help to advance the fault classification and prediction. On the one hand, the improved EMD can decompose the vibration signals into IMFs more efficiently and accurately to acquire more fault characteristic information prior to feature extraction. On the other hand, IMF can provide new feature choice besides time and frequency domain analysis. Currently, there are several methods to extract the features statistically from IMFs, e.g., EMD energy entropy [2], characteristic amplitude ratios [13], and Hilbert envelope spectrum [14]. These features have been successfully used to construct SVM or ANN-based expert system. In conclusion, both at signal-processing stage and feature-extraction stage, the improved EMD with ISBM will help to enhance the efficiency and accuracy.

6. Conclusion

The newly developed end effect restraint technique ISBM has been presented in this paper to improve the EMD method, and its performance compared with those of two other end condition methods. The proposed method, which showed its robust and effective end effect restraint ability, is heavily recommended for analysis of non-stationary, nonlinear signals. In addition, the industrial cases, as noted above, showed the potential of improved EMD for use in fault diagnosis of large rotating machinery, and that it is a promising new addition to existing toolboxes for non-stationary, nonlinear signal processing to the fault diagnosis of large rotating machinery.

Acknowledgments

The author would like to thank colleagues of Research Institute of Diagnostics and Cybernetics, Xi'an Jiaotong University for their kind support during the work of this paper.

References

[1] S. Sinclair, G.G.S. Pegram, Empirical mode decomposition in 2-D space and time: a tool for space–time rainfall analysis and nowcasting, *Hydrology and Earth System Sciences Discussions* 9 (3) (2005) 127–137.

[2] Yu Yang, Dejie Yu, Junsheng Cheng, A roller bearing fault diagnosis method based on EMD energy entropy and ANN, *Journal of Sound and Vibration* 294 (2006) 269–277.

[3] N.E. Huang, Introduction to the Hilbert–Huang transform and its related mathematical problems, *Interdisciplinary Mathematics* 5 (2005) 1–26.

[4] N.E. Huang, et al., The empirical mode decomposition and the Hilbert spectrum for nonlinear and non-stationary time series analysis, *Proceedings of the Royal Society of London Series A* 454 (1998) 903–995.
[5] Y.S. Zhang, J.W. Liang, J.X. Hu, The processing of end effects in EMD method by autoregressive model, *Progresses in Nature Science* 13 (2003) 1054–1059.
[6] Y.J. Deng, W. Wang, Boundary processing technique in EMD method and Hilbert transform, *Chinese Science Bulletin* 46 (2001) 257–263.
[7] L.S. Qu, G.H. Xu, One decade of holospectral technique: review and prospect, *Proceedings of the 1999 ASME Design Engineering Technical Conferences*, 1999, pp. 1–9.
[8] D.F. Shi, L.S. Qu, N.N. Gindy, General interpolated fast Fourier transform: a new tool for diagnosing large rotating machinery, *Journal of Vibration and Acoustics* 127 (2005) 351–361.
[9] K.T. Coughlin, K.K. Tung, 11-Year solar cycle in the stratosphere extracted by the empirical mode decomposition method, *Advances in Space Research* 34 (2004) 323–329.
[10] G. Rilling, P. Flandrin, P. Goncalves, On empirical mode decomposition and its algorithms, *IEEE-EURASIP Workshop on Nonlinear Signal and Image Processing*, NSIP-03, 2003, pp. 1–5.
[11] F.H.S. Chiew, M.C. Peel, G.E. Amirthanathan, G.G.S. Pegram, Identification of oscillations in historical global streamflow data using empirical mode decomposition, Seventh IAHS Scientific Assembly at Foz do Iguscu, Brazil, 2005, pp. 53–62.
[12] Marcus Dätig, Torsten Schlurmann, Performance and limitations of the Hilbert–Huang transformation (HHT) with an application to irregular water waves, *Ocean Engineering* 31 (2004) 1783–1834.
[13] Yu Yang, Dejie Yu, Junsheng Cheng, A fault diagnosis approach for roller bearing based on IMF envelope spectrum and SVM, *Measurement* 40 (2007) 943–950.
[14] Yaguo Lei, Zhengjia He, Yanyang Zi, Qiao Hu, Fault diagnosis of rotating machinery based on multiple ANFIS combination with GAs, *Mechanical Systems and Signal Processing* 21 (2007) 2280–2294.